Investigation of mode radiation loss for microdisk resonators with pedestals by FDTD technique

Yuede Yang (杨跃德)*, Shijiang Wang (王世江), and Yongzhen Huang (黄永箴)

State Key Laboratory on Integrated Optoelectronics, Institute of Semiconductors, Chinese Academy of Sciences, Beijing 100083, China

**E-mail: yyd@semi.ac.cn*

Received October 30, 2009

Mode radiation loss for microdisk resonators with pedestals is investigated by three-dimensional (3D) finite-difference time-domain (FDTD) technique. For the microdisk with a radius of 1 μm, a thickness of 0.2 μm, and a refractive index of 3.4, on a pedestal with a refractive index of 3.17, the mode quality (Q) factor of the whispering-gallery mode (WGM) quasi-$TE_{7,1}$ first increases with the increase of the radius of the pedestal, and then quickly decreases as the radius is larger than 0.75 μm. The mode radiation loss is mainly the vertical radiation loss induced by the mode coupling between the WGM and vertical radiation mode in the pedestal, instead of the scattering loss around the perimeter of the round pedestal. The WGM can keep the high Q factor when the mode coupling is forbidden.

OCIS codes: 140.3410, 140.5960.

doi: 10.3788/COL20100805.0502.

Semiconductor microdisk lasers[1] are extensively studied due to their advantages, such as ultrasmall volume and high quality factors. Although there are no real transverse electric (TE) and transverse magnetic (TM) modes in three-dimensional (3D) resonators, the modes in the microdisk resonators can be assigned as quasi-TE and quasi-TM modes based on their main polarization. Usually, the microdisk lasers are supported by pedestals to form the strong vertical waveguide, and quasi-TE modes are dominant modes in the microdisk. The finite-difference time-domain (FDTD) technique is widely used in the simulations of circular[2,3] and double-notched-shaped microdisk resonators[4], photonic crystal waveguides[5], although it still has a few deficiencies[6,7]. The simulated scattering loss of the pedestal is small for the microdisk with a small pedestal by a two-dimensional (2D) method, because the distribution of the whispering-gallery mode (WGM) is concentrated near the circumference[2]. However, the vertical radiation loss is neglected in the 2D simulation, and the decrease of quality (Q) factor is caused by the enhancement of the scattering loss in the horizontal plane. Recently, we have analyzed the mode characteristics for microcylinder resonators with weak vertical waveguide by 3D FDTD technique, and found that the quasi-TM modes can keep high Q factors[8] and a critical lateral size is required for obtaining the high Q factor quasi-TE modes[9]. In this letter, the influence of the pedestal on the mode characteristics is investigated by 3D FDTD technique.

A microdisk resonator, which is supported by a pedestal and surrounded by air, is simulated by 3D FDTD method[3]. Based on the circular symmetry, the 3D problem can be transformed into a 2D one with the angular field dependence of $\exp(\mathrm{i}v\varphi)$, here v is the azimuthal mode number. The quasi-TE modes in the microdisk resonators are marked as quasi-$TE_{v,l}$, where the subsuript l is the radial mode number. The radiation modes in the pedestal are marked as $HE_{v,l}$ and $EH_{v,l}$, here EH modes usually have a shorter cut-off wavelength than that of HE modes, so only HE modes are considered in this letter. Figure 1 shows the cross section of the microdisk with a calculating window bounded by Γ_a, Γ_b, Γ_c, and Γ_d. Here R_1 and R_2 are the radii of the microdisk and pedestal, d is the thickness of the center layer, n_1 and n_2 are the refractive indices of the microdisk and the pedestal, respectively. The refractive indices n_1 and n_2 are 3.4 and 3.17, which are close to those of InGaAsP and InP, respectively. The perfect matched layer (PML) absorbing boundary condition is applied on the boundaries Γ_a, Γ_b, and Γ_c, which are placed 1.0, 4.0, and 5.0 μm away from the microdisk's upper, lateral, and lower boundaries, respectively. We expect that the mode fields E_z and H_z are Bessel functions when r approaches zero[3]. The asymptote of the Bessel function as r approaches zero is $\psi(r) \propto r^v (v > 0)$. We apply the asymptote to the field components E_z and H_z at the inner boundary Γ_d at $r = 4\Delta r$. The spatial steps Δz and Δr are 10 and 20 nm, respectively, and the time step Δt is chosen to satisfy the Courant condition. In the FDTD simulation, an exciting source with a cosine impulse is added to one component of the electromagnetic at a point (x_0, y_0) inside the microdisk. The cosine impulse is modulated by a Gaussian function

$$P(x_0, y_0, t) = \exp[-(t - t_0)^2/t_\mathrm{w}^2] \cos(2\pi f t), \qquad (1)$$

where t_0 and t_w are the times of the pulse center and the pulse half width, respectively, and f is the center frequency of the pulse. Then the time variation of a selected field component at some points inside the microdisk is recorded as the FDTD output. The Padé approximation with Baker's algorithm[10]is used to transform the FDTD output from the time-domain to the frequency-domain and calculate the mode frequencies and Q factors. The mode frequency f_m and the Q factor are calculated from the peak position of the spectrum and the ratio of the frequency to the full-width at half-maximum (FWHM) of the peak as $\mathrm{Q} = f_\mathrm{m}/\Delta f$.

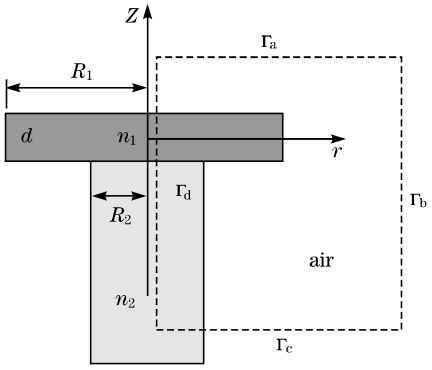

Fig. 1. Cross section of a microdisk with a pedestal and the calculation region.

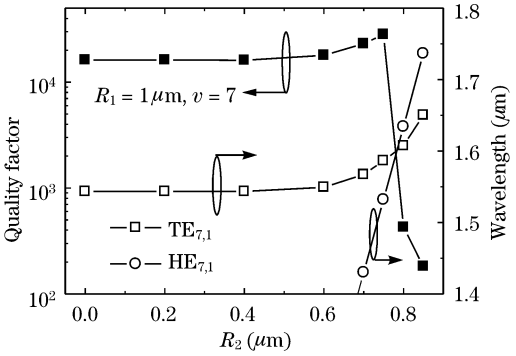

Fig. 2. Mode wavelength and Q factor of $TE_{7,1}$ mode versus the radius R_2 of the pedestal in the microdisk with $R_1 = 1$ μm and $d = 0.2$ μm. The cut-off wavelength of $HE_{7,1}$ mode is also plotted as open circles.

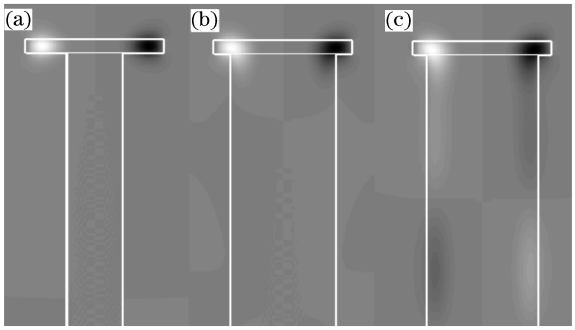

Fig. 3. Field patterns of magnetic field component H_z for $TE_{7,1}$ mode in the microdisk with $R_1 = 1$ μm and $d = 0.2$ μm obtained by FDTD simulation at (a) $R_2 = 0.4$ μm, (b) $R_2 = 0.75$ μm, and (c)$R_2 = 0.8$ μm.

For the microdisk with $R_1 = 1$ μm and $d = 0.2$ μm, the mode wavelength and Q factor of quasi-$TE_{7,1}$ mode are calculated and plotted versus R_2 in Fig. 2. The mode wavelength and Q factor keep constant values as $R_2 <$ 0.4 μm, because the pedestal is not large enough to superpose the main field intensity region of the WGM and has almost no influence on the mode characteristics. The mode wavelength increases from 1.543 to 1.650 μm as R_2 increases from 0.4 to 0.85 μm. The increases of the mode wavelength and Q factor with the increase of the pedestal can be understood as the result of the increase of the effective refractive index of the cavity, which is also observed in the square resonator with a pedestal[11]. The Q factor increases from 1.6×10^4 to 2.8×10^4 as R_2 increases from 0.4 to 0.75 μm, because the horizontal radiation loss decreases with the increase of the effective refractive index and the vertical radiation loss is still absent. Finally, the Q factor rapidly decreases to the order of 10^2 as R_2 > 0.75 μm. The cut-off wavelength of the vertical radiation mode $HE_{7,1}$ in the pedestal is also calculated and plotted in Fig. 2, which can be obtained as their vertical propagation constant $\beta = 0$. The mode wavelength can be obtained from the 2D eigenvalue equation

$$J_7(n_2kR_2)H_7^{\prime(2)}(kR_2) = n_2J_7'(n_2kR_2)H_7^{(2)}(kR_2), \quad (2)$$

where k is the wavenumber in vacuum, $J_7(x)$ is the J-type Bessel function of order 7, and $H_7^{(2)}(x)$ is the second-kind Hankel function of order 7[9]. We find that the mode wavelength of the WGM quasi-$TE_{7,1}$ mode is smaller than the cut-off wavelength of the vertical radiation mode $HE_{7,1}$ when R_2>0.75 μm, which means that the mode coupling can happen between the two modes. The mode coupling between the quasi-TE WGM and the vertical radiation mode in the pedestal results in a vertical radiation loss, and degrades the Q factor of WGM greatly. In the microcylinder resonators, the quasi-TE WGMs also have the high Q factors when their mode wavelengths are larger than the cut-off wavelengths of the vertical radiation HE modes[9]. The mode wavelength and Q factor of the microdisk with $R_2 > 0.9$ μm are not presented in Fig. 1, because the asymmetric structure cannot support TE guide mode when R_2 >0.9 μm.

In order to prove that the decrease of the Q factors is caused by the vertical radiation loss, we calculate the single mode field distribution using a long optical pulse with narrow bandwidth to excite only one mode by FDTD simulation. Figure 3 depicts the field patterns of magnetic field component H_z for quasi-$TE_{7,1}$ mode in the microdisk with $R_1 = 1$ μm and $d = 0.2$ μm. Figure 3(a) shows the field distribution in the microdisk with $R_2 = 0.4$ μm. The pedestal does not superpose the main field intensity region of the quasi-$TE_{7,1}$ mode, so the mode wavelength and Q factor of the quasi-$TE_{7,1}$ mode are the same with those in the microdisk without the pedestal. Figure 3(b) shows the field distribution in the microdisk with $R_2 = 0.75$ μm. Although the pedestal superpose the main field intensity region of the quasi-$TE_{7,1}$ mode, the vertical field distribution is still confined well, and the Q factor of the quasi-$TE_{7,1}$ mode is even larger than that in the microdisk without the pedestal because the horizontal loss decreases. Figure 3(c) shows the field distribution in the microdisk with $R_2 = 0.8$ μm. The field distribution oscillates in the pedestal, corresponding to the vertical radiation loss, so the Q factor of the quasi-$TE_{7,1}$ mode is very small. Conclusively, the variation of the field distributions verifies that the vertical radiation loss degrades the mode Q factor of the quasi-$TE_{7,1}$ mode when the mode wavelength of quasi-$TE_{7,1}$ mode is smaller than the cut-off wavelength of the vertical radiation mode $HE_{7,1}$.

To verify that the results presented above are general, we also calculate the mode wavelength and Q factor for the quasi-$TE_{9,1}$ WGM in the microdisk with $R_1 = 1.2$ μm

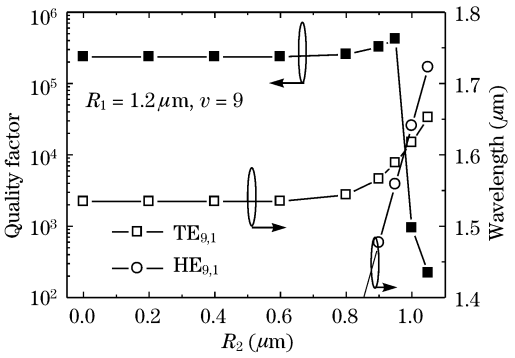

Fig. 4. Mode wavelength and Q factor of $TE_{9,1}$ mode versus the radius R_2 of the pedestal in the microdisk with $R_1 = 1.2$ μm and $d = 0.2$ μm. The cut-off wavelength of $HE_{9,1}$ mode is also plotted as open circles.

and $d = 0.2$ μm, and plot the results in Fig. 4. The cut-off wavelength of the vertical radiation mode $HE_{9,1}$ in the pedestal is also calculated and plotted in Fig. 4. The mode wavelength first keeps a constant value as $R_2 < 0.6$ μm, and then increases from 1.535 to 1.652 μm as R_2 increases from 0.6 to 1.05 μm. The Q factor also first keeps a constant value as $R_2 < 0.6$ μm, and then increases from 2.4×10^5 to 4.2×10^5 as R_2 increases from 0.6 to 0.95 μm, finally rapidly decreases to the order of 10^2 as $R_2 > 0.95$ μm. The variations of the mode wavelength and Q factor for the quasi-$TE_{9,1}$ WGM are similar to those for the quasi-$TE_{7,1}$ mode. The results show that the mode coupling between the WGM and the vertical radiation mode is a common phenomenon for the microdisk resonators, which will induce the vertical radiation loss and degrade the Q factor of WGMs.

In conclusion, we have investigated the mode characteristics for the 3D microdisk resonators with pedestals by 3D FDTD simulation. The mode coupling between the quasi-TE WGM and the vertical radiation mode is observed. The mode coupling results in the vertical radiation loss for the quasi-TE WGMs and degrades the mode Q factors. The results also show that the overlap of the pedestal and mode field distribution does not induce the scattering loss, and the quasi-TE WGMs can keep the high Q factors when the pedestal size is smaller than a critical value to keep the mode wavelengths larger than that of the corresponding vertical radiation modes.

This work was supported by the National Natural Science Foundation of China (Nos. 60777028, 60723002, and 60838003), the Major State Basic Research Program (No. 2006CB302804), and the Project of National Lab for Tsinghua Information Technologies.

References

1. S. L. McCall, A. F. J. Levi, R. E. Slusher, S. J. Pearton, and R. A. Logan, Appl. Phys. Lett. **60,** 289 (1992).
2. M. Fujita, A. Sakai, and T. Baba, IEEE J. Sel. Top. Quantum Electron. **5,** 673 (1999).
3. B. J. Li and P. L. Liu, IEEE J. Quantum Electron. **32,** 1583 (1996).
4. X. Luo and A. W. Poon, Chin. Opt. Lett. **7,** 296 (2009).
5. Z. Yong, H. Fu, X. Qiao, Y. Li, D. Zhao, and P. Ge, Acta Opt. Sin. (in Chinese) **29,** 1070 (2009).
6. J. Niegemann, W. Pernice, and K. Busch, J. Opt. A: Pure Appl. Opt. **11,** 114015 (2009).
7. A. I. Nosich, E. I. Smotrova, S. V. Boriskina, T. M. Benson, and P. Sewell, Opt. Quantum Electron. **39,** 1253 (2007).
8. Y. D. Yang, Y. Z. Huang, and Q. Chen, Phys. Rev. A **75,** 013817 (2007).
9. Y. Z. Huang and Y. D. Yang, J. Lightwave Technol. **26,** 1411 (2008).
10. W. H. Guo, W. J. Li, and Y. Z. Huang, IEEE Microw. Wirel. Compon. Lett. **11,** 223 (2001).
11. Q. Chen and Y. Z. Huang, J. Opt. Soc. Am. B **23,** 1287 (2006).